NASA
Technical
Paper
2539

February 1986

Breakdown of the Conservative Potential Equation

M. D. Salas and
Clyde R. Gumbert

NASA

NASA
Technical
Paper
2539

1986

Breakdown of the Conservative Potential Equation

M. D. Salas and
Clyde R. Gumbert

Langley Research Center
Hampton, Virginia

National Aeronautics
and Space Administration

Scientific and Technical
Information Branch

Summary

The conservative full-potential equation is used to study transonic flow over five airfoil sections. The results of the study indicate that once shock waves are present in the flow, the qualitative behavior of the potential approximation is different from that observed with the Euler equations. The difference in behavior for the potential equation approximation eventually leads to multiple solutions.

Introduction

The first step in obtaining a mathematical description of a physical process consists of deciding what physical features of the problem are important. A danger usually lurks at this stage. Too often, physically important features are not included in the mathematical model because their inclusion could render the problem mathematically intractable. In this paper, the physical process to be modeled is the flow of air at transonic speed past a two-dimensional wing section. If the airfoil shape considered is aerodynamically efficient and shock waves are not too strong, then viscous effects are confined to a thin layer near the surface of the airfoil. As a first approximation to the flow field, the effect of this layer on the flow is neglected. Next, the flow is assumed to have a steady state; thus, only the steady-state part of the governing equations is considered. The steady-state assumptions seem reasonable within the constraints of an aerodynamically efficient shape and weak shock waves. But, the problem is still governed by three nonlinear partial differential equations—the steady-state Euler equations. What else can be done to simplify the mathematical complexity? If the flow is subsonic and the upstream far field is uniform, the flow will be irrotational and isentropic. Since only weak shock waves are considered, perhaps the irrotational and isentropic assumptions can be used in the transonic range and still allow a satisfactory approximation to the flow field. Under these assumptions, the problem is reduced to its simplest form—a nonlinear second-order partial differential equation and two algebraic relations. How far into the transonic regime can we push this model and still get "meaningful" results? Meaningful, in the present context, means at least qualitative agreement with the next more accurate model, that is, the steady-state Euler equations. The answer to this question is the main subject of this paper.

It is already known, from the work reported in references 1 and 2, that if the shock becomes too strong, the conservative potential model produces the anomalous results shown in figure 1. It is also known from reference 2 that the shock strength has to be measured relative to the thickness of the airfoil, not, as previously thought, in some absolute sense by requiring that $(M_u^2 - 1)^3 \ll 1.3$. (The symbol M_u represents the Mach number upstream of the shock wave.) It was unfortunate, however, that in both references the emphasis in the anomalous behavior was placed on its nonunique character. The association of the anomalous behavior with multiple solutions (e.g., the existence of three possible solutions at zero angle of attack, as shown in fig. 1) could be taken to mean that one of the solutions was "meaningful" and that the problem could be resolved by developing some criteria that would single out this solution. In figure 1, the nonlifting solution has the desirable quality of being symmetrical; therefore, this solution was considered valid. It was, therefore, felt that the problem was somehow connected with "lift." As we now understand the problem, these notions are erroneous. In this paper, we show that the nonuniqueness problem of the conservative potential model is an indication of a breakdown of the model and that none of the solutions available in this range are meaningful. To obtain meaningful solutions, the model must be modified.

To accomplish the objectives just discussed, a data base covering a wide range of Mach numbers and angles of attack in the subsonic and transonic domain was created for the following airfoils:

NACA 0012	Reference 3 (p. A1-6)
KORN 75-06-12	Reference 4 (pp. 96–101)
NLR 7301	Reference 3 (p. A4-7)
RAE 2822	Reference 3 (p. A6-9)
NACA 65-213	Reference 5

These particular airfoils were chosen because of their wide use for both research and practical applications. The airfoil profiles, shown in figure 2, are defined in the references given next to each designated airfoil in the list above. Of the airfoils studied, the NLR 7301 and the KORN 75-06-12 are designed for shockless supercritical flow conditions.

As part of this study, we mapped the region in the angle-of-attack, Mach number (α, M_∞) plane where the conservative potential model qualitatively begins to depart from the behavior expected of the Euler equations. That is, we established the onset of breakdown for these five airfoils. It is expected that the results obtained with these particular airfoils can be used as a guide when dealing with other airfoil profiles.

Symbols

a speed of sound

b	constant in equation (11)
c	constant in equation (11)
c_d	section drag coefficient
c_l	section lift coefficient
F	airfoil section shape
M	Mach number
$\mathbf{n}$	unit normal to shock wave
$\mathbf{V}$	velocity
x, y	Cartesian coordinates of some point P
α	angle of attack
α_0	angle of attack for which $\partial c_l/\partial M_\infty = 0$
β	compressibility factor, $(1 - M_\infty^2)^{1/2}$
Γ	circulation
γ	ratio of specific heats
ρ	density
Φ	potential

Subscripts:

d	downstream of shock wave
u	upstream of shock wave
∞	free-stream value

Governing Equations

Following the approach set forth in the Introduction, we consider here the equations governing the flow of a perfect gas past an airfoil profile defined by $F(x, y) = 0$. If the flow is irrotational, it satisfies the condition

$$\nabla \times \mathbf{V} = 0 \tag{1}$$

which can be identically satisfied by introducing a potential function, Φ, such that

$$\mathbf{V} = \nabla \Phi \tag{2}$$

The equation governing the flow expresses the conservation of mass

$$\nabla \cdot (\rho \nabla \Phi) = 0 \tag{3}$$

The appropriate shock jump condition consistent with the conservation of mass is

$$\mathbf{n} \cdot [\![\rho \nabla \Phi]\!] = 0 \tag{4}$$

where $\mathbf{n}$ is the unit normal to the shock wave. To guarantee that the jump condition (eq. (4)) is satisfied across shock waves, it is necessary to write the discrete analog of equation (3) in divergence form. Finally, the equation for the conservation of total energy

$$a^2 + \frac{\gamma - 1}{2} |\nabla \Phi|^2 = a_0^2 \tag{5}$$

(where a_0 is constant) and the isentropic relation

$$\left(\frac{a}{a_\infty}\right)^2 = \left(\frac{\rho}{\rho_\infty}\right)^{\gamma - 1} \tag{6}$$

provide the required relationship between the density and the potential function Φ.

The boundary condition at the surface of the airfoil is

$$\nabla F \cdot \nabla \Phi = 0 \tag{7}$$

while in the far field, the potential should have the following asymptotic behavior:

$$\Phi \xrightarrow[x^2+y^2 \to \infty]{} V_\infty \left[x \cos \alpha + y \sin \alpha + \frac{\Gamma}{2\pi} \tan^{-1} \left(\frac{\beta y}{x} \right) \right] \tag{8}$$

The symbol Γ represents the circulation which must be found as part of the solution to the problem by requiring that the velocity at a sharp trailing edge remains finite.

It must be emphasized that the above mathematical description of the flow, which we will call the conservative potential model, is one of several possible approximations to the full Euler equations. For example, another model could retain the mass conservation equation and the isentropic relation but not require the flow to be irrotational or to conserve total energy. Such a model, which we will call the isentropic Euler model, was used by Magnus and Yoshihara (ref. 6) for transonic flow calculations. The problem with the isentropic Euler model is that it is as difficult to solve as the full Euler equations model. However, as evident from figure 3, it does represent the shock jump better than the conservative potential model; there are indications (see ref. 7) that it does not have the anomalous behavior of the conservative potential model.

The governing equations are mapped to the "circle plane," where they are solved by the finite-volume, multigrid technique described in references 1, 8, and 9. The numerical code embodying these techniques is known as FLO 36. The reader is referred to references 1 and 2 for a description of the many numerical experiments already performed which show that the nonuniqueness is admitted by the differential system of equations, independent of the discretization procedure.

Results and Discussion

All results reported for the conservative potential model were obtained by running FLO 36 with a fine grid consisting of 192 mesh points around the airfoil and 32 mesh points between the airfoil and the far field. In all cases, the fine mesh residual was reduced by at least five orders of magnitude from its initial value. The solutions were obtained by specifying the lift coefficient and Mach number and computing the angle of attack and drag coefficient. In most cases, the incompressible solution was used to start the iterative process. However, for high-lift cases where convergence was not as swift, the iterative process was started from the converged solution at a lower lift coefficient. The results for lift and wave drag as a function of M_∞ and α are tabulated in the appendix.

Lift curves for each airfoil section at various free-stream Mach numbers are shown in figure 4. Each lift curve was generated from about 20 individual calculations by using a cubic spline under tension. It is obvious that the nonuniqueness problem occurs throughout the angle-of-attack, Mach number plane, not as previously thought "in certain bands of angle of attack and Mach number" (ref. 1). It is interesting to note that for the cambered airfoil sections, the point where all the lift curves come together, usually known as the "zero-lift incidence" point, does not occur at zero lift for the Mach numbers shown. According to the Prandtl-Glauert rule,

$$\frac{\partial c_l}{\partial M_\infty} = \frac{M_\infty}{\beta^2} c_l \tag{9}$$

and since this point corresponds to $\partial c_l/\partial M_\infty = 0$, it follows that at this point $c_l = 0$. As the Mach number decreases, the "zero-lift incidence" point does drift to $c_l = 0$. At present it is not clear if the discrepancy is a numerical inaccuracy or some nonlinear effect not accounted for by the Prandtl-Glauert rule. Let us focus on a particular lift curve, for example figure 4(e), $M_\infty = 0.720$, and investigate its behavior in some detail. Starting from the point where $\partial c_l/\partial M_\infty = 0$ and moving in the direction of increasing α, the lift initially shows the expected linear increase with α, then shows a faster rate of increase. The curve eventually develops into the multivalued "S"-shape. The upper part of the S-shaped curve, where the slope is again positive, corresponds to the upper airfoil surface shock wave reaching the airfoil trailing edge. Once the shock wave reaches the trailing edge, it cannot be properly resolved with the "O" mesh used in FLO 36. For this reason, most of the lift curves shown in figure 4 do not reach this point. Beyond this point there is a decrease in the rate of lift produced by the airfoil because of the increasing size of the supersonic bubble on the lower surface of the airfoil. The loci of points at different free-stream Mach numbers corresponding to maximum absolute lift form an envelope in the c_l, α plane.

Figure 5 shows the wave drag curves for the same cases. Figure 5 can be used to estimate the formation of shock waves by determining the points where the wave drag departs from zero. The maximum wave drag envelope corresponds to the maximum lift envelope of figure 4.

Let us again look at the lift-curve behavior. Figures 6 and 7 show the lift curves for an NACA 0012 airfoil at $M_\infty = 0.67$ and 0.75, respectively. In these two figures, the conservative potential results from FLO 36 are compared with the Euler results obtained with FLO 52MG (ref. 10). At the lower Mach number (fig. 6), the agreement between the potential and the Euler solutions is excellent up to approximately $\alpha = 3.5°$. Figure 5(a) shows that at this point, the wave drag starts to increase. The deviation, therefore, between the potential and the Euler solutions for α greater than 3.5° is caused by the presence of the shock wave. A similar observation can be made at $M_\infty = 0.75$ (fig. 7), except that the deviation now starts at about $\alpha = 1.5°$. Figure 8 compares the angles made by the lift curves for the cases shown in figures 6 and 7. The angle is plotted as a function of c_l to avoid the multivalue behavior associated with α. The figure shows that before shock waves are developed, the lift behaves as predicted by linear theory, that is,

$$c_l \approx \frac{2\pi\alpha}{\beta} \tag{10}$$

Once a shock wave is present, the qualitative behavior of the conservative potential and the Euler models is different. The behavior of the potential model when a shock wave is formed and shortly after is approximately

$$\frac{\partial c_l}{\partial \alpha} = \tan(bc_l + c) \tag{11}$$

where b and c are constants. This behavior corresponds to the regions on either side of the minimum in figure 9. From equation (11), we can determine that the lift now increases exponentially with α. It is this behavior, which as we have seen starts as soon as shock waves are developed, that eventually leads to the nonuniqueness problem. The nonuniqueness problem is, therefore, not a sudden occurrence, but rather a manifestation of the weakness of the conservative potential model in handling shock waves. A price had to be paid for the simplicity of the model.

Figure 10 shows that the behavior observed in figure 8 is universal. Some of the spikes shown in the curves of figure 10 are spurious oscillations generated by the spline interpolating routine. The sudden drop observed at the high c_l values is not caused by any defects in the spline. It is consistent with the S-shaped curve.

Finally, in figure 11, the region in the α, M_∞ plane where the conservative potential model qualitatively deviates from the behavior of the Euler model is mapped for the five airfoils under investigation. The criterion used for this purpose was the point at which $\partial c_l/\partial\alpha$ was no longer constant. Shown in figure 11 are the design points for shockless supercritical flow conditions for the KORN 75-06-12 and the NLR 7301 airfoils. Both design points fall outside of the onset of breakdown. A detailed investigation of flow conditions in the neighborhood of these two design points reveals that they are isolated shockless solutions surrounded by solutions with shocks. Table I gives the approximated values of α_0 used in figure 11.

TABLE I. VALUES OF ZERO-LIFT INCIDENCE ANGLE

Airfoil	α_0, deg
KORN 75-06-12	−2.25
NLR 7301	−2.30
RAE 2822	−1.70
NACA 65-213	−1.95

Implications and Recommendations

The breakdown of the conservative potential model is expected to be somewhat masked when the approximation is used in conjunction with viscous-inviscid interaction techniques, since the viscous effects tend to decrease the strength of the shock and move it upstream. The occurrence of strong shocks, in whose presence the breakdown becomes more apparent, generally causes the viscous interaction to become more difficult to solve as well. However, the symptoms of the breakdown, of which the most obvious is the steepening of the lift curve, appear before the shock becomes strong enough to affect the viscous interaction adversely.

To extend the usefulness of the conservative potential model, it is recommended that the treatment of shock waves in the model be modified to account for some rotational effects, as discussed in reference 7. An alternative is to use a nonconservative formulation. In that case, a more comprehensive evaluation of the nonconservative potential equation than that presented in reference 2 is required.

Concluding Remarks

The inviscid flow over five airfoil sections was investigated in detail by using the conservative full-potential equation in the transonic range. It was shown that once a shock wave is present, the qualitative behavior of the potential and Euler models is different. It is this difference in the treatment of shock waves that eventually leads to the nonuniqueness problem. A map of the region in the angle-of-attack, Mach number (α, M_∞) plane showing where the conservative potential model begins to deviate from the Euler model was presented for the five airfoils investigated.

NASA Langley Research Center
Hampton, VA 23665-5225
November 7, 1985

Appendix

Calculated Lift and Wave-Drag Coefficients

NACA 0012

$M_\infty = 0.670$

α, deg	c_l	c_d
-5.259	-1.298	0.0706
-4.886	-1.101	0.0443
-4.353	-0.903	0.0226
-3.640	-0.704	0.0076
-2.740	-0.504	0.0008
-1.689	-0.303	0.0000
-0.581	-0.104	0.0000
0.540	0.096	0.0000
1.650	0.296	0.0000
2.704	0.496	0.0007
3.611	0.696	0.0072
4.331	0.896	0.0219
4.870	1.094	0.0434
5.248	1.291	0.0696
5.485	1.487	0.0985

$M_\infty = 0.690$

α, deg	c_l	c_d
-4.600	-1.297	0.0760
-4.350	-1.101	0.0506
-3.943	-0.903	0.0285
-3.356	-0.704	0.0117
-2.961	-0.597	0.0057
-2.573	-0.504	0.0023
-2.314	-0.446	0.0011
-1.574	-0.296	0.0000
-0.784	-0.146	0.0000
-0.019	-0.004	0.0000
0.784	0.146	0.0000
1.574	0.296	0.0000
2.314	0.446	0.0011
2.961	0.597	0.0057
3.496	0.746	0.0148
3.923	0.896	0.0278
4.247	1.044	0.0439
4.479	1.192	0.0622
4.630	1.340	0.0819
4.710	1.487	0.1023

$M_\infty = 0.710$

α, deg	c_l	c_d
-3.960	-1.297	0.0823
-3.739	-1.100	0.0567
-3.467	-0.902	0.0347
-3.015	-0.704	0.0168
-2.691	-0.597	0.0096
-2.364	-0.504	0.0050
-1.931	-0.396	0.0016
-0.994	-0.196	0.0000
-0.018	-0.004	0.0000
0.994	0.196	0.0000
1.931	0.396	0.0016
2.691	0.597	0.0096
3.246	0.796	0.0245
3.612	0.994	0.0446
3.814	1.192	0.0678
3.885	1.388	0.0924
3.854	1.584	0.1177
3.760	1.778	0.1433
3.660	1.971	0.1699

$M_\infty = 0.730$

α, deg	c_l	c_d
-2.915	-0.902	0.0411
-2.784	-0.803	0.0314
-2.605	-0.703	0.0226
-2.378	-0.604	0.0150
-2.098	-0.504	0.0089
-1.740	-0.397	0.0041
-0.922	-0.196	0.0002
-0.017	-0.004	0.0000
0.922	0.196	0.0002
1.740	0.397	0.0041
2.358	0.596	0.0146
2.770	0.796	0.0308
2.998	0.994	0.0508
3.078	1.191	0.0728
3.050	1.387	0.0957
2.963	1.582	0.1194
2.922	1.774	0.1457

$M_\infty = 0.750$

α, deg	c_l	c_d
-2.271	-1.576	0.1259
-2.213	-1.385	0.0995
-2.284	-1.190	0.0774
-2.307	-0.993	0.0566
-2.212	-0.795	0.0372
-1.952	-0.596	0.0204
-1.490	-0.397	0.0078
-0.818	-0.197	0.0013
-0.016	-0.004	0.0000
0.818	0.197	0.0013
1.490	0.397	0.0078
1.952	0.596	0.0204
2.212	0.795	0.0372
2.307	0.993	0.0566
2.284	1.190	0.0774
2.213	1.385	0.0995
2.271	1.576	0.1259

$M_\infty = 0.770$

α, deg	c_l	c_d
-1.556	-0.991	0.0624
-1.571	-0.794	0.0437
-1.458	-0.596	0.0268
-1.337	-0.496	0.0193
-1.164	-0.396	0.0129
-0.939	-0.297	0.0077
-0.661	-0.197	0.0038
-0.338	-0.096	0.0015
-0.013	-0.004	0.0007
0.338	0.096	0.0015
0.661	0.197	0.0038
0.939	0.297	0.0077
1.164	0.396	0.0129
1.337	0.496	0.0193
1.458	0.596	0.0268
1.535	0.695	0.0349
1.571	0.794	0.0437
1.575	0.893	0.0529
1.556	0.991	0.0624
1.510	1.187	0.0831

NACA 0012

$M_\infty = 0.790$

α, deg	c_l	c_d
-0.855	-0.988	0.0697
-0.868	-0.793	0.0504
-0.874	-0.595	0.0336
-0.747	-0.396	0.0191
-0.439	-0.197	0.0085
-0.009	-0.004	0.0045
0.439	0.197	0.0085
0.747	0.396	0.0191
0.874	0.595	0.0336
0.868	0.793	0.0504
0.855	0.988	0.0697

$M_\infty = 0.810$

α, deg	c_l	c_d
-0.265	-0.789	0.0593
-0.229	-0.594	0.0415
-0.243	-0.396	0.0276
-0.163	-0.196	0.0179
-0.003	-0.004	0.0144
0.163	0.196	0.0179
0.243	0.396	0.0276
0.229	0.594	0.0415
0.265	0.789	0.0593

$M_\infty = 0.820$

α, deg	c_l	c_d
0.052	-0.592	0.0476
0.045	-0.493	0.0405
0.017	-0.395	0.0345
-0.005	-0.295	0.0296
-0.015	-0.196	0.0259
-0.011	-0.096	0.0236
-0.000	-0.004	0.0229
0.011	0.096	0.0236
0.015	0.196	0.0259
0.005	0.295	0.0296
-0.017	0.395	0.0345
-0.045	0.493	0.0405
-0.052	0.592	0.0476
0.014	0.689	0.0562

$M_\infty = 0.670$

α, deg	c_l	c_d
-7.153	-1.566	0.1957
-7.073	-1.378	0.1520
-6.895	-1.188	0.1099
-6.598	-0.994	0.0717
-6.161	-0.798	0.0401
-5.563	-0.600	0.0169
-4.781	-0.400	0.0037
-3.806	-0.200	0.0000
-2.713	0.000	0.0000
-1.590	0.200	0.0000
-0.466	0.400	0.0000
0.638	0.600	0.0001
1.676	0.800	0.0014
2.564	1.000	0.0056
3.249	1.200	0.0142
3.726	1.401	0.0278
4.010	1.601	0.0479
4.120	1.799	0.0744
4.065	1.995	0.1050
3.846	2.189	0.1365
3.474	2.382	0.1650

$M_\infty = 0.700$

α, deg	c_l	c_d
-5.920	-1.559	0.2038
-5.935	-1.371	0.1673
-5.893	-1.182	0.1282
-5.754	-0.991	0.0899
-5.489	-0.796	0.0554
-5.071	-0.599	0.0277
-4.471	-0.400	0.0094
-3.668	-0.200	0.0013
-2.693	0.000	0.0000
-1.651	0.200	0.0000
-0.603	0.400	0.0000
0.415	0.600	0.0002
1.327	0.800	0.0016
2.021	1.000	0.0063
2.460	1.201	0.0169
2.665	1.401	0.0358
2.652	1.599	0.0612
2.426	1.795	0.0890
2.027	1.988	0.1140

$M_\infty = 0.720$

α, deg	c_l	c_d
-5.171	-1.553	0.2021
-5.168	-1.365	0.1729
-5.176	-1.177	0.1392
-5.125	-0.987	0.1030
-4.969	-0.794	0.0680
-4.671	-0.598	0.0378
-4.200	-0.400	0.0158
-3.529	-0.200	0.0038
-2.668	0.000	0.0002
-1.696	0.200	0.0000
-0.710	0.400	0.0000
0.239	0.600	0.0002
1.038	0.800	0.0016
1.545	1.001	0.0079
1.764	1.201	0.0238
1.720	1.399	0.0471
1.428	1.595	0.0726
1.054	1.788	0.0954

$M_\infty = 0.740$

α, deg	c_l	c_d
-4.705	-1.547	0.1986
-4.496	-1.360	0.1731
-4.462	-1.171	0.1463
-4.457	-0.982	0.1152
-4.391	-0.791	0.0819
-4.209	-0.597	0.0505
-3.868	-0.399	0.0251
-3.338	-0.200	0.0085
-2.617	-0.000	0.0012
-1.746	0.200	0.0000
-0.835	0.400	0.0000
0.022	0.600	0.0002
0.653	0.800	0.0023
0.902	1.001	0.0149
0.831	1.199	0.0362
0.484	1.395	0.0594
0.311	1.588	0.0821

$M_\infty = 0.760$

α, deg	c_l	c_d
-4.462	-1.445	0.1873
-3.969	-1.260	0.1600
-3.815	-1.071	0.1366
-3.782	-0.881	0.1100
-3.768	-0.786	0.0952
-3.738	-0.690	0.0800
-3.682	-0.593	0.0648
-3.595	-0.496	0.0504
-3.469	-0.398	0.0372
-3.301	-0.299	0.0257
-3.088	-0.200	0.0162
-2.828	-0.100	0.0091
-2.524	0.000	0.0042
-1.799	0.200	0.0003
-1.012	0.400	0.0005
-0.265	0.600	0.0011
0.052	0.800	0.0097
-0.033	0.999	0.0287
-0.384	1.194	0.0499

$M_\infty = 0.780$

α, deg	c_l	c_d
-3.653	-1.158	0.1504
-3.264	-0.970	0.1275
-3.189	-0.875	0.1168
-3.153	-0.780	0.1052
-3.131	-0.685	0.0925
-3.108	-0.589	0.0790
-3.069	-0.492	0.0652
-3.005	-0.395	0.0516
-2.908	-0.298	0.0388
-2.774	-0.199	0.0275
-2.601	-0.100	0.0181
-2.390	0.000	0.0109
-1.884	0.200	0.0037
-1.362	0.400	0.0051
-1.023	0.600	0.0135
-1.018	0.798	0.0274
-1.128	0.993	0.0452

$M_\infty = 0.790$

α, deg	c_l	c_d
-2.977	-0.872	0.1186
-2.889	-0.777	0.1083
-2.845	-0.682	0.0972
-2.819	-0.586	0.0852
-2.794	-0.490	0.0723
-2.754	-0.393	0.0592
-2.691	-0.296	0.0464
-2.599	-0.198	0.0347
-2.475	-0.099	0.0246
-2.150	0.100	0.0115
-1.799	0.300	0.0089
-1.610	0.499	0.0165
-1.740	0.696	0.0320
-1.398	0.892	0.0449

$M_\infty = 0.795$

α, deg	c_l	c_d
-2.913	-0.870	0.1195
-2.782	-0.775	0.1094
-2.716	-0.680	0.0991
-2.682	-0.584	0.0879
-2.657	-0.489	0.0757
-2.627	-0.392	0.0630
-2.580	-0.295	0.0504
-2.510	-0.197	0.0388
-2.414	-0.099	0.0287
-2.295	0.000	0.0207
-1.926	0.300	0.0133
-1.874	0.400	0.0165
-1.893	0.498	0.0220
-1.950	0.597	0.0287
-1.941	0.695	0.0359
-1.673	0.793	0.0423
-1.650	0.800	0.0423

$M_\infty = 0.800$

α, deg	c_l	c_d
-2.501	-0.391	0.0668
-2.470	-0.294	0.0547
-2.422	-0.196	0.0433
-2.354	-0.098	0.0334
-2.272	0.001	0.0256
-2.187	0.100	0.0204
-2.115	0.200	0.0182
-2.081	0.299	0.0191
-2.108	0.399	0.0228
-2.188	0.497	0.0282
-2.023	0.693	0.0397

$M_\infty = 0.620$

α, deg	c_l	c_d
-6.755	-0.803	0.0252
-5.961	-0.604	0.0108
-5.019	-0.404	0.0030
-3.958	-0.204	0.0002
-2.833	-0.004	-0.0001
-1.690	0.196	-0.0001
-0.547	0.396	0.0000
0.581	0.596	0.0001
1.659	0.796	0.0022
2.634	0.996	0.0076
3.461	1.196	0.0175
4.131	1.396	0.0324
4.647	1.595	0.0526
5.023	1.794	0.0784
5.270	1.991	0.1108
5.396	2.186	0.1489
5.409	2.378	0.1900
5.315	2.568	0.2314
5.111	2.758	0.2710
4.809	2.947	0.3064

$M_\infty = 0.650$

α, deg	c_l	c_d
-6.187	-0.803	0.0333
-5.571	-0.604	0.0148
-4.790	-0.404	0.0047
-3.852	-0.204	0.0007
-3.339	-0.103	0.0000
-2.810	-0.004	-0.0001
-2.274	0.096	-0.0001
-1.196	0.296	-0.0001
-0.127	0.496	-0.0001
0.900	0.696	0.0010
1.817	0.896	0.0045
2.213	0.996	0.0077
2.863	1.197	0.0181
3.332	1.397	0.0345
3.636	1.597	0.0585
3.790	1.794	0.0901
3.803	1.988	0.1260
3.684	2.181	0.1628
3.438	2.373	0.1975

$M_\infty = 0.680$

α, deg	c_l	c_d
-5.474	-0.802	0.0521
-5.055	-0.604	0.0234
-4.470	-0.404	0.0077
-3.703	-0.204	0.0014
-2.777	-0.004	0.0000
-2.284	0.096	-0.0001
-1.785	0.196	-0.0001
-1.286	0.296	-0.0001
-0.789	0.396	-0.0001
-0.300	0.496	0.0000
0.624	0.696	0.0009
1.381	0.897	0.0044
1.908	1.097	0.0139
2.224	1.298	0.0326
2.352	1.496	0.0603
2.310	1.691	0.0922
2.109	1.885	0.1241
1.782	2.077	0.1529
1.603	2.173	0.1660
1.451	2.269	0.1788

$M_\infty = 0.700$

α, deg	c_l	c_d
-4.994	-1.504	0.2176
-5.068	-1.304	0.1766
-5.081	-1.085	0.1331
-4.995	-0.895	0.0904
-4.783	-0.701	0.0527
-4.423	-0.504	0.0231
-3.892	-0.304	0.0062
-3.556	-0.204	0.0025
-2.743	-0.004	0.0000
-1.822	0.196	0.0000
-0.892	0.396	0.0000
-0.001	0.596	0.0002
0.733	0.796	0.0020
1.194	0.997	0.0113
1.418	1.197	0.0321
1.434	1.364	0.0599
1.263	1.589	0.0893
0.946	1.782	0.1167
0.776	1.878	0.1293
0.643	1.974	0.1419

$M_\infty = 0.720$

α, deg	c_l	c_d
-4.166	-1.446	0.2244
-4.202	-1.261	0.1908
-4.273	-1.076	0.1528
-4.289	-0.888	0.1124
-4.203	-0.697	0.0728
-3.982	-0.502	0.0387
-3.602	-0.304	0.0137
-3.346	-0.204	0.0060
-2.687	-0.004	0.0003
-1.865	0.196	0.0000
-1.018	0.396	0.0000
-0.212	0.596	0.0000
0.314	0.797	0.0052
0.553	0.996	0.0226
0.549	1.194	0.0476
0.335	1.389	0.0743
0.174	1.486	0.0870
0.007	1.583	0.0991
-0.098	1.679	0.1115

$M_\infty = 0.740$

α, deg	c_l	c_d
-3.480	-1.251	0.1984
-3.472	-1.065	0.1677
-3.529	-0.879	0.1328
-3.547	-0.690	0.0952
-3.459	-0.499	0.0589
-3.230	-0.303	0.0285
-2.836	-0.104	0.0081
-1.912	0.200	0.0002
-0.884	0.500	0.0036
-0.588	0.600	0.0050
-0.403	0.700	0.0102
-0.302	0.799	0.0183
-0.314	0.997	0.0401
-0.695	1.289	0.0755
-0.810	1.382	0.0873
-0.748	1.478	0.1005

$M_\infty = 0.750$

α, deg	c_l	c_d
-3.504	-1.336	0.2161
-3.167	-1.153	0.1870
-3.125	-0.967	0.1575
-3.178	-0.781	0.1241
-3.194	-0.592	0.0880
-3.106	-0.399	0.0534
-2.878	-0.203	0.0250
-2.493	-0.004	0.0071
-2.245	0.096	0.0030
-1.675	0.297	0.0030
-1.153	0.496	0.0092
-0.806	0.696	0.0194
-0.815	0.893	0.0390
-1.041	1.088	0.0611
-1.138	1.282	0.0838

$M_\infty = 0.760$

α, deg	c_l	c_d
-3.275	-1.237	0.2050
-2.867	-1.054	0.1764
-2.795	-0.869	0.1483
-2.839	-0.682	0.1163
-2.855	-0.492	0.0819
-2.773	-0.299	0.0491
-2.561	-0.103	0.0235
-2.406	-0.003	0.0147
-2.027	0.196	0.0069
-1.648	0.396	0.0119
-1.358	0.595	0.0230
-1.342	0.792	0.0398
-1.519	0.988	0.0599
-1.391	1.181	0.0819

NLR 7301

$M_\infty = 0.770$

α, deg	c_l	c_d
-4.170	-1.313	0.2355
-3.076	-1.139	0.1952
-2.592	-0.956	0.1670
-2.484	-0.770	0.1401
-2.514	-0.583	0.1096
-2.537	-0.393	0.0773
-2.478	-0.199	0.0476
-2.323	-0.003	0.0262
-2.114	0.196	0.0172
-1.947	0.395	0.0214
-1.951	0.593	0.0358
-1.997	0.789	0.0519
-1.855	0.983	0.0699

$M_\infty = 0.780$

α, deg	c_l	c_d
-2.190	-0.578	0.1193
-2.243	-0.388	0.0903
-2.272	-0.196	0.0631
-2.257	-0.001	0.0428
-2.243	0.196	0.0340
-2.309	0.394	0.0368
-2.479	0.590	0.0483
-2.348	0.785	0.0631

$M_\infty = 0.800$

α, deg	c_l	c_d
-1.818	-0.565	0.1395
-1.778	-0.377	0.1216
-1.955	-0.187	0.1062
-2.251	0.005	0.0954
-2.615	0.197	0.0902
-2.816	0.390	0.0869

$M_\infty = 0.630$

α, deg	c_l	c_d
-7.267	-1.000	0.0250
-6.521	-0.799	0.0098
-5.589	-0.600	0.0023
-4.492	-0.400	0.0000
-3.314	-0.200	0.0000
-2.107	0.000	0.0000
-1.499	0.100	0.0000
-0.890	0.200	0.0000
-0.282	0.300	0.0000
0.325	0.400	0.0000
0.927	0.500	0.0000
1.523	0.600	0.0000
2.688	0.800	0.0001
3.767	1.000	0.0021
4.680	1.200	0.0093
5.390	1.400	0.0228
5.930	1.599	0.0427
6.310	1.797	0.0690
6.550	1.994	0.1009
6.670	2.189	0.1357
6.680	2.383	0.1720

$M_\infty = 0.660$

α, deg	c_l	c_d
-6.642	-0.999	0.0359
-6.079	-0.800	0.0123
-5.317	-0.600	0.0027
-4.341	-0.400	0.0001
-3.240	-0.200	0.0000
-2.098	0.000	0.0000
-1.520	0.100	0.0000
-0.942	0.200	0.0000
-0.364	0.300	0.0000
0.211	0.400	0.0000
0.781	0.500	0.0000
1.343	0.600	0.0000
2.433	0.800	0.0000
3.403	1.000	0.0019
4.150	1.200	0.0094
4.675	1.400	0.0242
5.012	1.600	0.0468
5.187	1.798	0.0749
5.216	1.994	0.1056
5.111	2.189	0.1369
4.876	2.383	0.1668

$M_\infty = 0.690$

α, deg	c_l	c_d
-5.875	-0.996	0.0559
-5.504	-0.800	0.0248
-4.945	-0.600	0.0051
-4.149	-0.400	0.0003
-3.149	-0.200	0.0000
-2.621	-0.100	0.0000
-2.084	0.000	0.0000
-1.543	0.100	0.0000
-1.000	0.200	0.0000
-0.459	0.300	0.0000
0.080	0.400	0.0000
1.134	0.600	0.0000
2.131	0.800	0.0000
2.940	1.000	0.0023
3.468	1.200	0.0127
3.760	1.400	0.0321
3.854	1.598	0.0567
3.770	1.795	0.0834
3.521	1.991	0.1097
3.107	2.186	0.1335

$M_\infty = 0.710$

α, deg	c_l	c_d
-5.366	-1.376	0.1403
-5.373	-1.185	0.1060
-5.275	-0.993	0.0710
-5.033	-0.798	0.0384
-4.611	-0.600	0.0130
-3.969	-0.400	0.0008
-2.578	-0.100	0.0000
-2.072	0.000	0.0000
-1.559	0.100	0.0000
-1.044	0.200	0.0000
-0.530	0.300	0.0000
-0.021	0.400	0.0000
0.970	0.600	0.0000
1.872	0.800	0.0002
2.518	1.000	0.0053
2.866	1.200	0.0200
2.969	1.399	0.0410
2.860	1.596	0.0648
2.558	1.792	0.0886
2.172	1.987	0.1132

$M_\infty = 0.730$

α, deg	c_l	c_d
-4.637	-1.371	0.1478
-4.613	-1.180	0.1168
-4.601	-0.989	0.0852
-4.482	-0.795	0.0537
-4.199	-0.598	0.0257
-3.707	-0.400	0.0068
-2.516	-0.100	0.0005
-2.051	0.000	0.0001
-1.575	0.100	0.0000
-1.093	0.200	0.0000
-0.612	0.300	0.0000
-0.138	0.400	0.0000
0.758	0.600	0.0003
1.479	0.800	0.0036
1.921	1.000	0.0136
2.058	1.199	0.0309
1.928	1.397	0.0519
1.570	1.593	0.0737

$M_\infty = 0.750$

α, deg	c_l	c_d
-3.926	-1.365	0.1493
-3.853	-1.175	0.1237
-3.872	-0.984	0.0970
-3.851	-0.791	0.0686
-3.699	-0.596	0.0408
-3.359	-0.399	0.0181
-2.414	-0.100	0.0027
-2.008	0.000	0.0013
-1.582	0.100	0.0005
-1.148	0.200	0.0001
-0.717	0.300	0.0002
-0.301	0.400	0.0006
0.415	0.600	0.0036
0.876	0.800	0.0121
1.026	1.026	0.0267
0.869	1.197	0.0453

$M_\infty = 0.770$

α, deg	c_l	c_d
-3.325	-1.169	0.1292
-3.176	-0.978	0.1056
-3.165	-0.883	0.0937
-3.162	-0.786	0.0814
-3.150	-0.690	0.0688
-3.113	-0.592	0.0561
-3.038	-0.495	0.0438
-2.919	-0.397	0.0324
-2.748	-0.298	0.0225
-2.522	-0.199	0.0147
-2.243	-0.100	0.0090
-1.923	0.000	0.0052
-1.578	0.100	0.0030
-1.228	0.200	0.0020
-0.892	0.300	0.0023
-0.589	0.400	0.0040
-0.158	0.600	0.0116
-0.053	0.799	0.0248
-0.275	0.996	0.0423

$M_\infty = 0.790$

α, deg	c_l	c_d
-2.616	-0.876	0.1019
-2.532	-0.781	0.0913
-2.493	-0.685	0.0806
-2.472	-0.588	0.0696
-2.441	-0.491	0.0585
-2.388	-0.394	0.0475
-2.301	-0.296	0.0372
-2.172	-0.197	0.0279
-2.005	-0.099	0.0204
-1.808	0.001	0.0147
-1.598	0.100	0.0112
-1.394	0.200	0.0099
-1.221	0.300	0.0107
-1.104	0.400	0.0136
-1.060	0.499	0.0183
-1.101	0.599	0.0246
-1.214	0.698	0.0322
-1.347	0.795	0.0409

RAE 2822

$M_\infty = 0.800$

α, deg	c_l	c_d
-2.507	-0.873	0.1059
-2.324	-0.778	0.0954
-2.222	-0.682	0.0854
-2.168	-0.586	0.0753
-2.136	-0.489	0.0652
-2.103	-0.392	0.0550
-2.053	-0.294	0.0452
-1.979	-0.196	0.0361
-1.878	-0.098	0.0285
-1.761	0.002	0.0227
-1.641	0.101	0.0192
-1.540	0.200	0.0179
-1.484	0.300	0.0190
-1.491	0.400	0.0222
-1.569	0.498	0.0273
-1.697	0.597	0.0339

$M_\infty = 0.810$

α, deg	c_l	c_d
-2.987	-0.961	0.1240
-2.264	-0.774	0.0999
-1.927	-0.583	0.0806
-1.832	-0.389	0.0625
-1.792	-0.194	0.0458
-1.739	0.003	0.0338
-1.729	0.102	0.0307
-1.755	0.201	0.0298
-1.831	0.300	0.0312
-1.958	0.399	0.0345

$M_\infty = 0.690$

α, deg	c_l	c_d
-5.708	-1.590	0.1295
-5.691	-1.396	0.0966
-5.557	-1.200	0.0651
-5.286	-1.003	0.0377
-4.852	-0.803	0.0176
-4.222	-0.603	0.0061
-3.379	-0.403	0.0012
-2.372	-0.204	0.0000
-1.311	-0.004	0.0000
-0.245	0.196	0.0000
0.798	0.396	0.0001
1.770	0.596	0.0015
2.615	0.796	0.0065
3.260	0.995	0.0192
3.709	1.193	0.0390
3.927	1.389	0.0657
3.946	1.582	0.0969

$M_\infty = 0.720$

α, deg	c_l	c_d
-4.422	-1.586	0.1324
-4.535	-1.393	0.1045
-4.575	-1.198	0.0757
-4.495	-1.002	0.0478
-4.262	-0.804	0.0237
-3.840	-0.604	0.0074
-3.185	-0.403	0.0011
-2.299	-0.204	0.0000
-1.332	-0.004	0.0000
-0.377	0.196	0.0006
0.503	0.396	0.0037
1.243	0.596	0.0117
1.793	0.794	0.0258
2.110	0.991	0.0467
2.221	1.186	0.0718
2.181	1.380	0.0981
2.147	1.571	0.1235
2.391	1.761	0.1491

$M_\infty = 0.750$

α, deg	c_l	c_d
-3.445	-1.194	0.0855
-3.531	-1.000	0.0604
-3.537	-0.901	0.0479
-3.506	-0.803	0.0358
-3.434	-0.704	0.0246
-3.313	-0.604	0.0149
-3.138	-0.504	0.0072
-2.902	-0.404	0.0023
-2.597	-0.303	0.0003
-2.217	-0.204	0.0002
-1.811	-0.104	0.0006
-1.407	-0.004	0.0016
-0.656	0.196	0.0064
-0.048	0.395	0.0163
0.359	0.594	0.0320
0.559	0.790	0.0519
0.601	0.984	0.0738
0.675	1.177	0.0957
1.143	1.367	0.1193

$M_\infty = 0.770$

α, deg	c_l	c_d
-2.752	-1.190	0.0911
-2.810	-0.996	0.0685
-2.859	-0.899	0.0572
-2.891	-0.801	0.0458
-2.890	-0.702	0.0347
-2.850	-0.603	0.0243
-2.761	-0.504	0.0152
-2.620	-0.404	0.0081
-2.419	-0.304	0.0038
-2.152	-0.204	0.0028
-1.845	-0.104	0.0038
-1.536	-0.004	0.0063
-0.989	0.196	0.0152
-0.618	0.394	0.0294
-0.447	0.590	0.0477
-0.381	0.785	0.0674
-0.143	0.978	0.0869
0.617	1.168	0.1102

NACA 65-213

$M_\infty = 0.790$

α, deg	c_l	c_d
-2.185	-0.895	0.0664
-2.215	-0.797	0.0564
-2.259	-0.699	0.0467
-2.290	-0.601	0.0373
-2.292	-0.502	0.0288
-2.255	-0.403	0.0217
-2.175	-0.303	0.0166
-2.052	-0.204	0.0141
-1.897	-0.104	0.0144
-1.743	-0.004	0.0167
-1.477	0.194	0.0279
-1.341	0.391	0.0440
-1.237	0.586	0.0615
-0.827	0.779	0.0792
0.485	0.966	0.1063

$M_\infty = 0.800$

α, deg	c_l	c_d
-1.924	-0.795	0.0628
-1.989	-0.599	0.0459
-2.045	-0.402	0.0321
-1.992	-0.204	0.0247
-1.862	-0.005	0.0264
-1.807	0.094	0.0303
-1.764	0.193	0.0362
-1.732	0.291	0.0433
-1.691	0.388	0.0511
-1.611	0.486	0.0591
-1.434	0.583	0.0672
-1.119	0.679	0.0758
-0.635	0.774	0.0862
0.352	0.865	0.1034

$M_\infty = 0.810$

α, deg	c_l	c_d
-1.937	-0.888	0.0788
-1.783	-0.791	0.0712
-1.707	-0.695	0.0635
-1.718	-0.597	0.0567
-1.771	-0.499	0.0505
-1.832	-0.401	0.0453
-1.887	-0.303	0.0414
-1.930	-0.204	0.0390
-1.960	-0.105	0.0385
-1.986	-0.006	0.0398
-2.026	0.190	0.0469
-1.916	0.386	0.0584
-1.358	0.579	0.0732
0.279	0.765	0.1004

References

1. Steinhoff, John; and Jameson, Antony: Multiple Solutions of the Transonic Potential Flow Equation. *A Collection of Technical Papers—AIAA 5th Computational Fluid Dynamics Conference*, June 1981, pp. 347–353. (Available as AIAA-81-1019.)
2. Salas, M. D.; Jameson, A.; and Melnik, R. E.: *A Comparative Study of the Nonuniqueness Problem of the Potential Equation.* NASA TP-2385, 1985. (Available as AIAA-83-1888.)
3. *Experimental Data Base for Computer Program Assessment.* AGARD-AR-138, May 1979.
4. Bauer, Frances; Garabedian, Paul; Korn, David; and Jameson, Antony: *Supercritical Wing Sections II. Volume 108 of Lecture Notes in Economics and Mathematical Systems,* Springer-Verlag, 1975.
5. Plentovich, E. B.; Ladson, Charles L.; and Hill, Acquilla S.: *Tests of a NACA 65_1-213 Airfoil in the NASA Langley 0.3-Meter Transonic Cryogenic Tunnel.* NASA TM-85732, 1984.
6. Magnus, R.; and Yoshihara, H.: Inviscid Transonic Flow Over Airfoils. *AIAA J.,* vol. 8, no. 12, Dec. 1970, pp. 2157–2162.
7. Hafez, M.; and Lovell, D.: Entropy and Vorticity Corrections for Transonic Flows. *A Collection of Technical Papers—AIAA 6th Computational Fluid Dynamics Conference,* July 1983, pp. 630–644. (Available as AIAA-83-1926.)
8. Jameson, Antony; and Caughey, D. A.: A Finite Volume Method for Transonic Potential Flow Calculations. *A Collection of Technical Papers—AIAA 3rd Computational Fluid Dynamics Conference,* June 1977, pp. 35–54. (Available as AIAA Paper 77-635.)
9. Jameson, Antony: Acceleration of Transonic Potential Flow Calculations on Arbitrary Meshes by the Multiple Grid Method. *A Collection of Technical Papers—AIAA Computational Fluid Dynamics Conference,* July 1979, pp. 122–146. (Available as AIAA Paper 79-1458.)
10. Jameson, Antony: *Solution of the Euler Equations for Two Dimensional Transonic Flow by a Multigrid Method.* MAE Report No. 1613, Princeton Univ., June 1983.

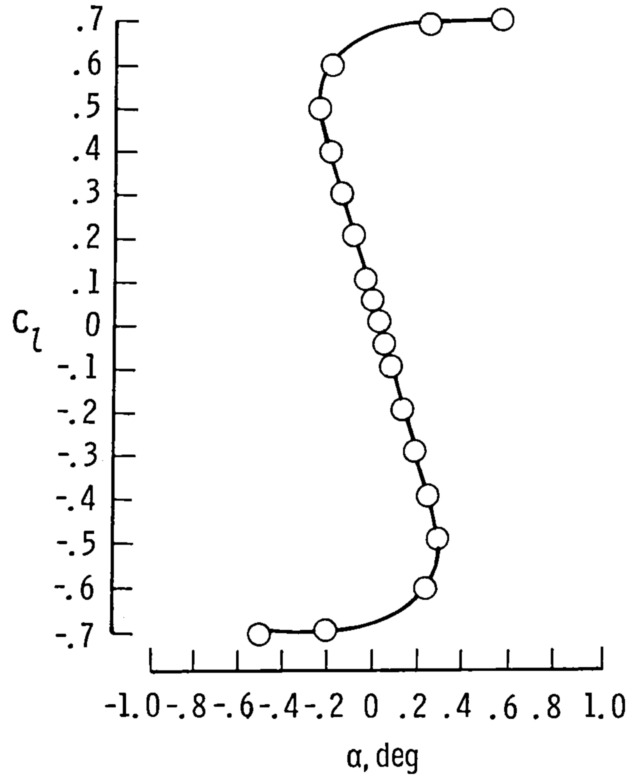

Figure 1. Multiple solutions for NACA 0012 airfoil section at $M_\infty = 0.83$ computed with FLO 36.

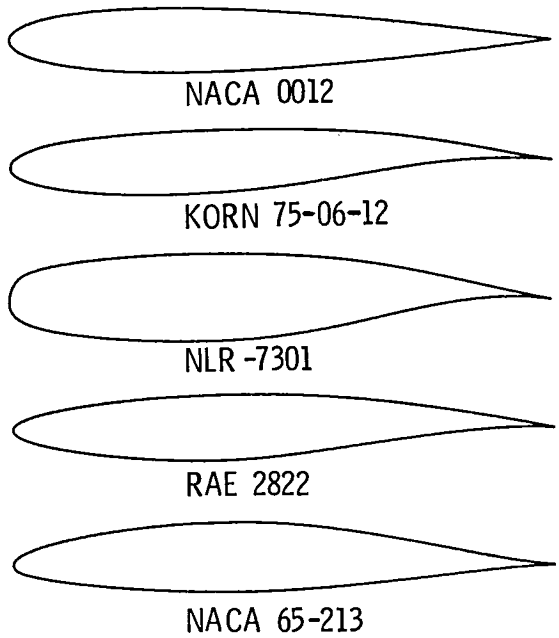

Figure 2. Airfoil sections under investigation.

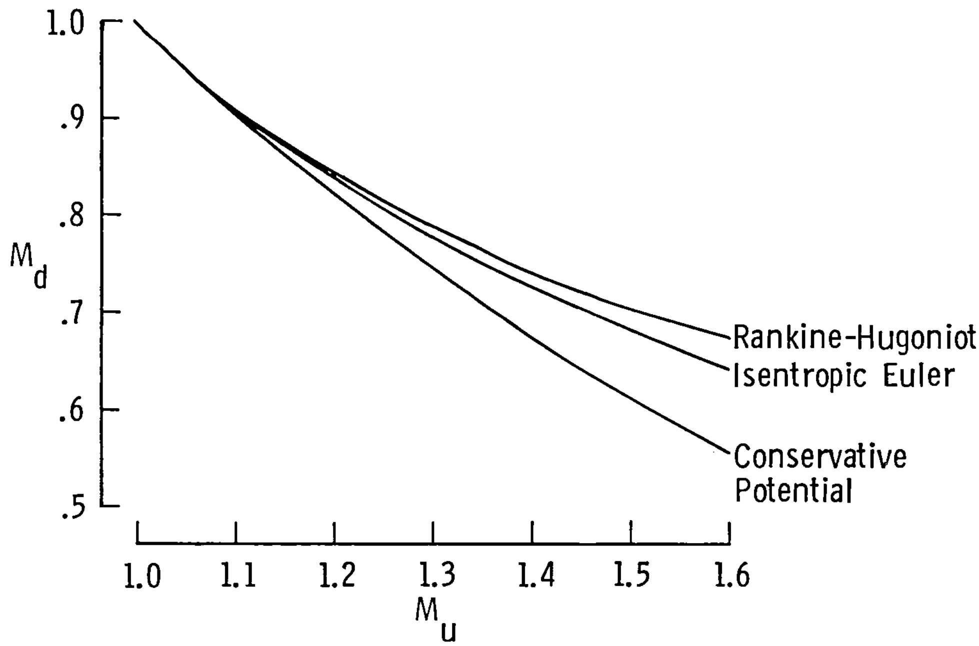

Figure 3. Shock jump conditions predicted by various inviscid models.

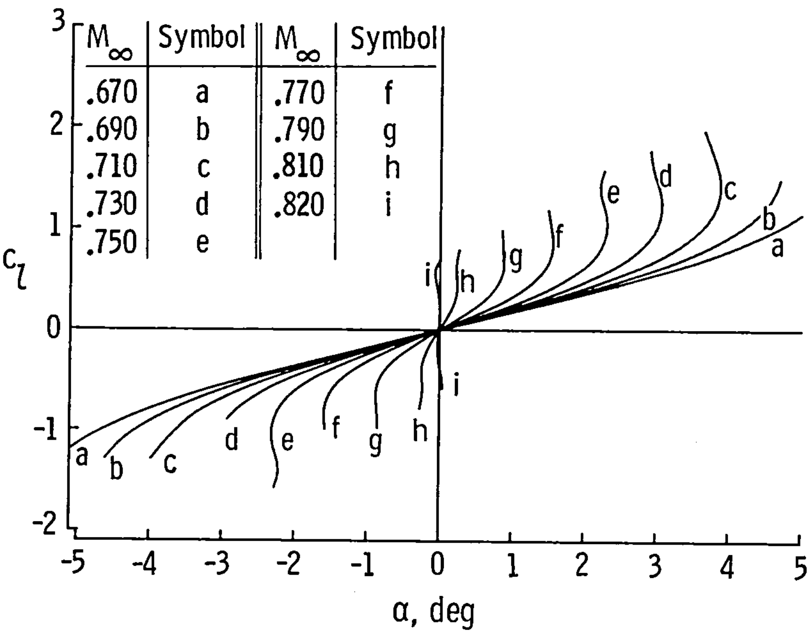

(a) NACA 0012.

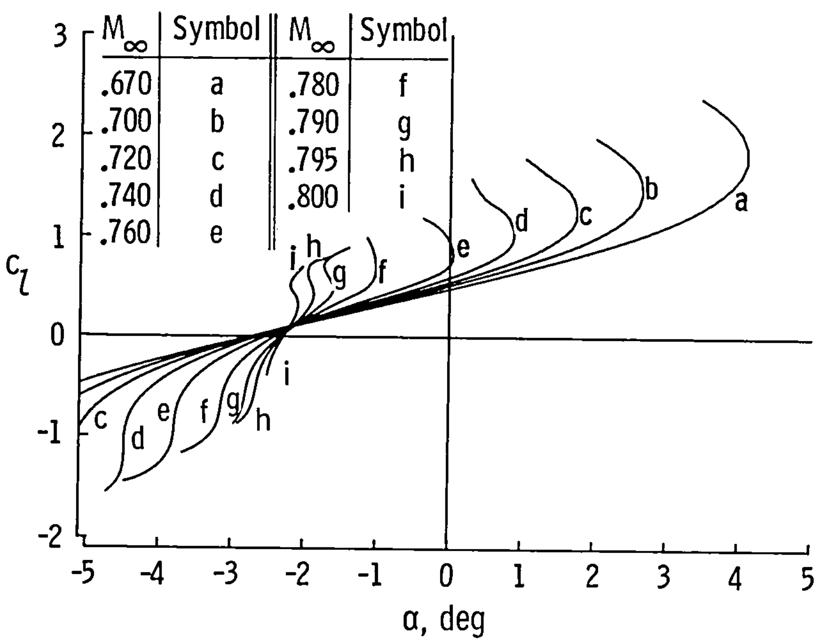

(b) KORN 75-06-12.

Figure 4. Lift curves computed with FLO 36.

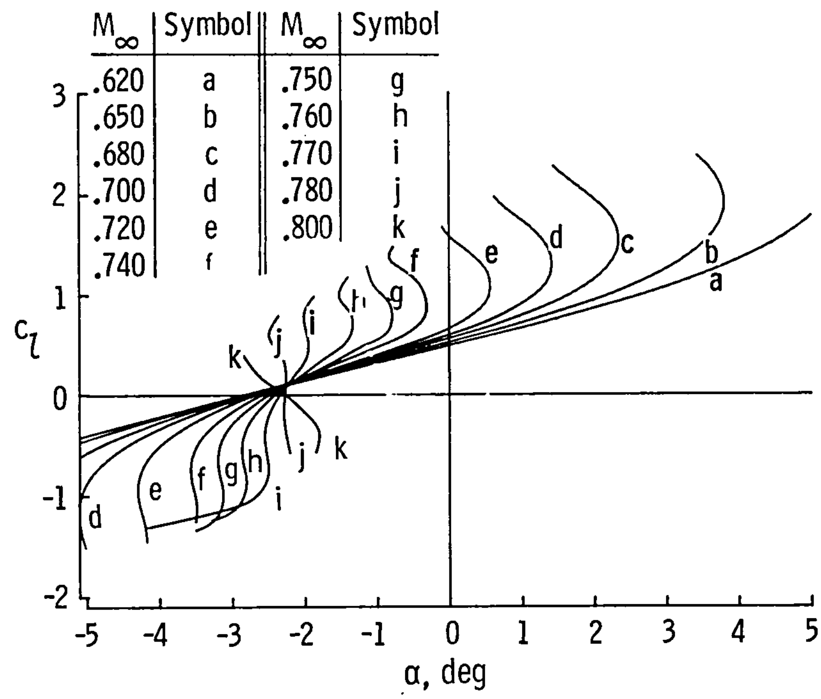

(c) NLR 7301.

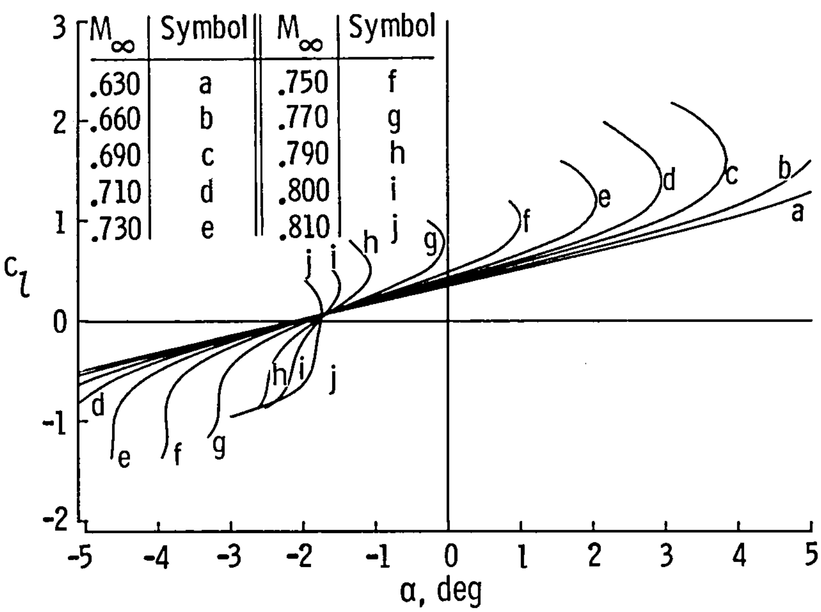

(d) RAE 2822.

Figure 4. Continued.

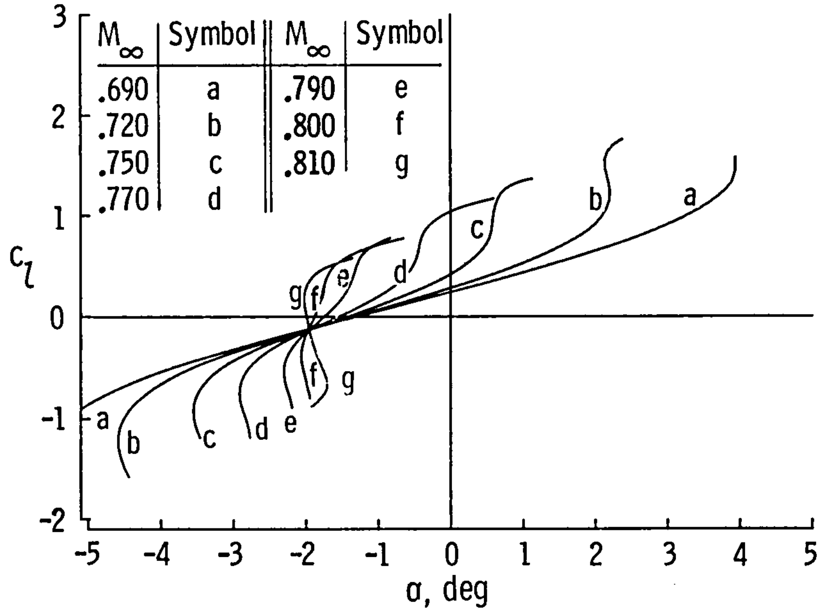

(e) NACA 65-213.

Figure 4. Concluded.

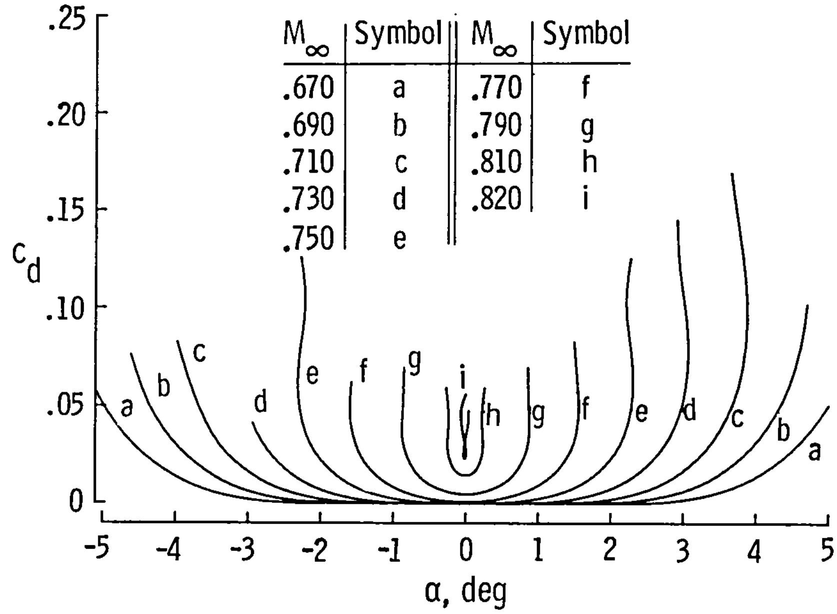

(a) NACA 0012.

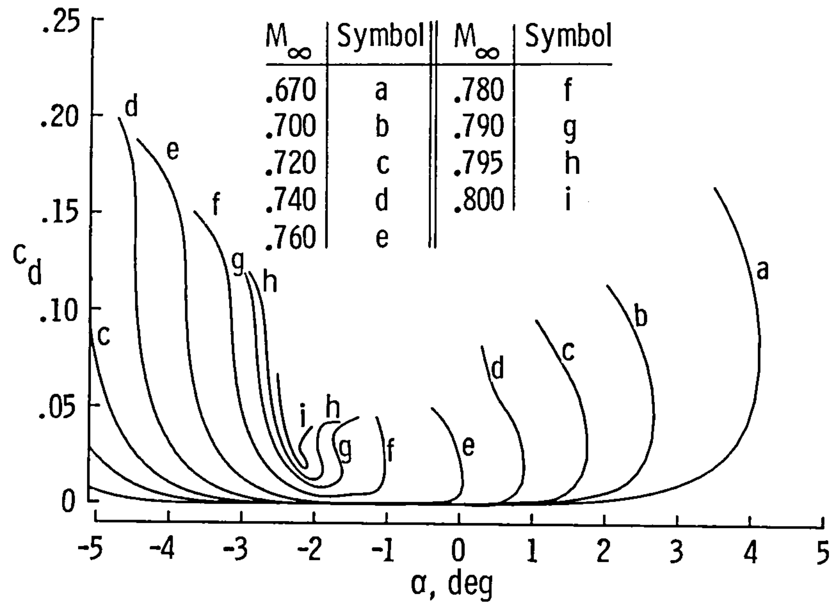

(b) KORN 75-06-12.

Figure 5. Drag curves computed with FLO 36.

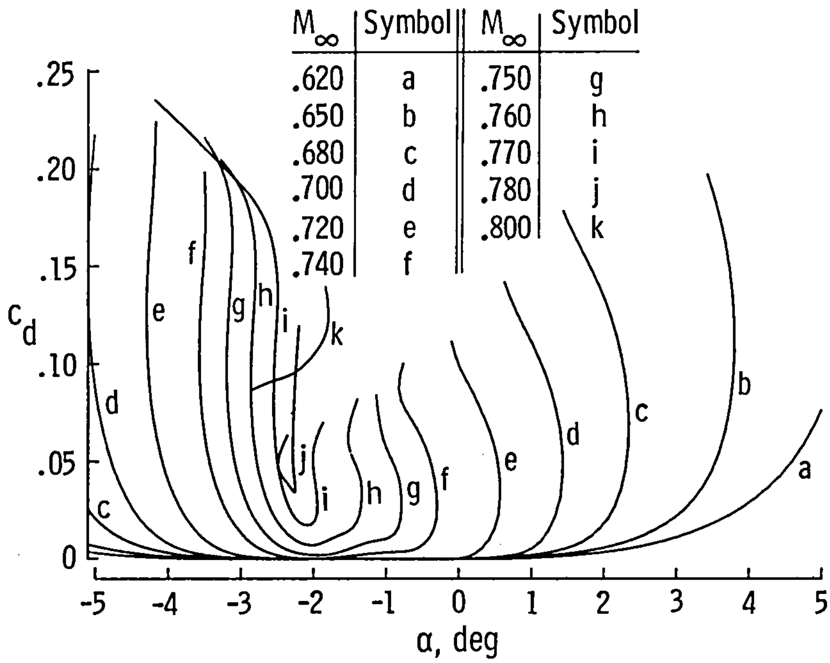

(c) NLR 7301.

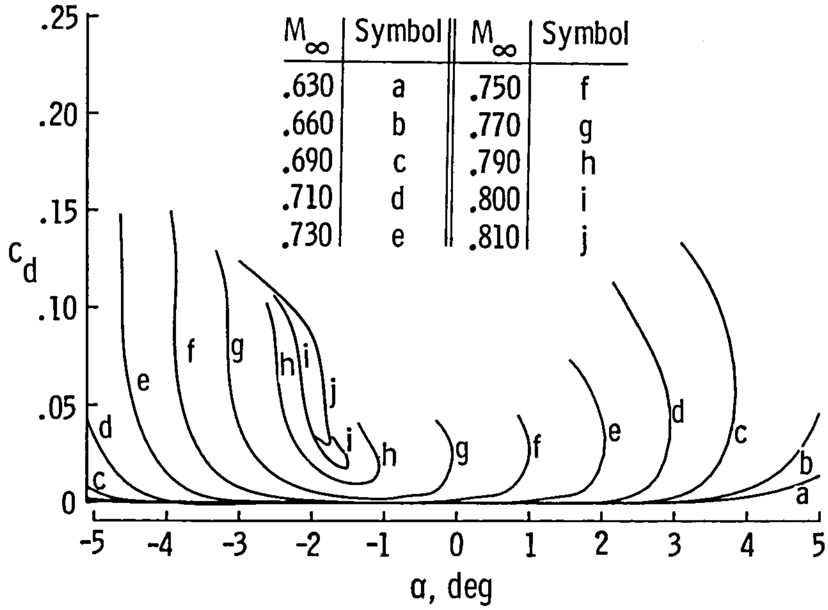

(d) RAE 2822.

Figure 5. Continued.

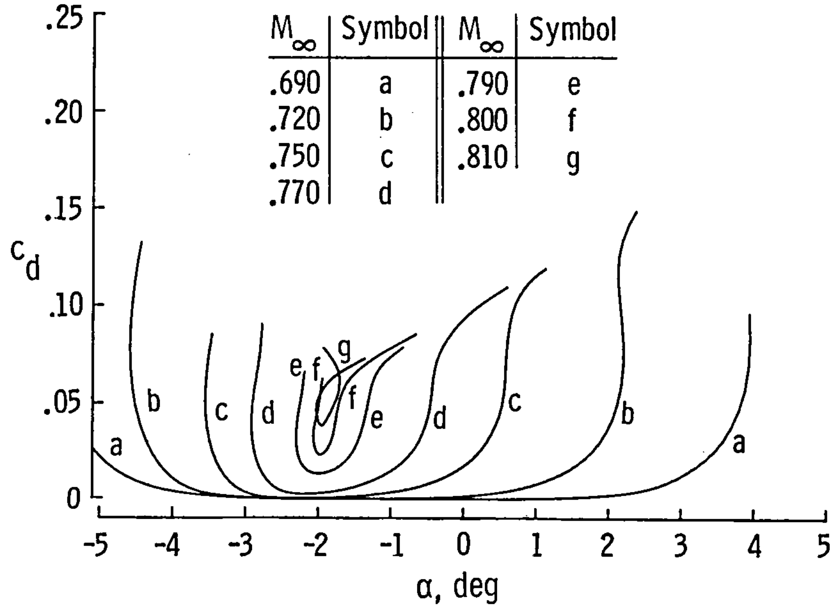

(e) NACA 65-213.

Figure 5. Concluded.

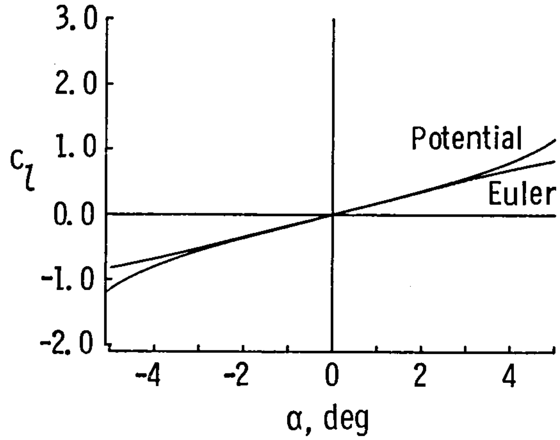

Figure 6. Details of lift curve for NACA 0012 section at $M_\infty = 0.67$ computed with FLO 36 and FLO 52MG.

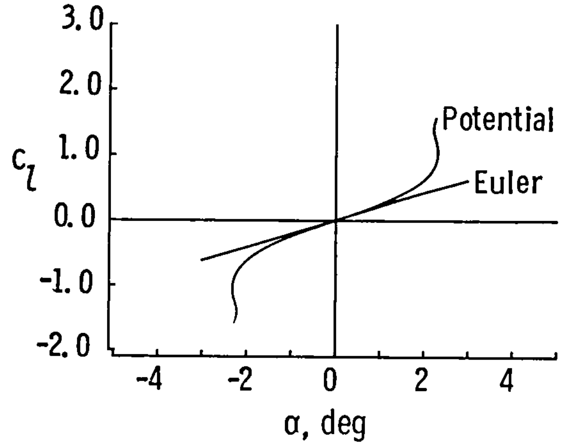

Figure 7. Details of lift curve for NACA 0012 section at $M_\infty = 0.75$ computed with FLO 36 and FLO 52MG.

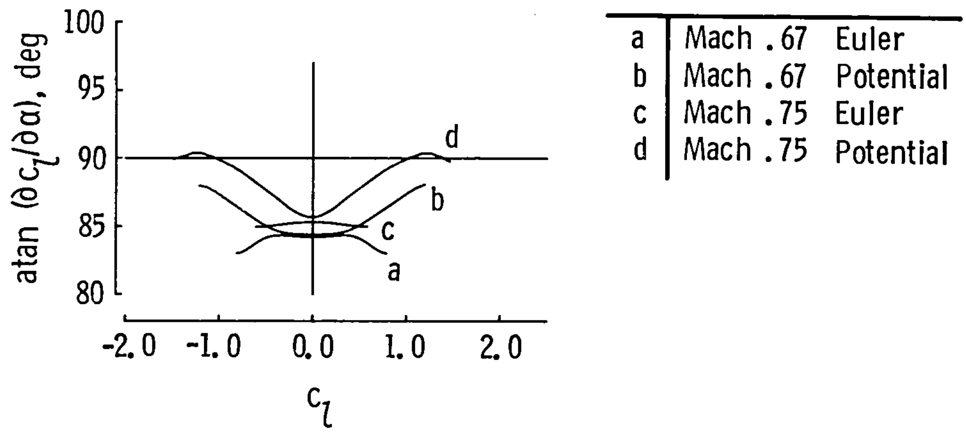

Figure 8. Behavior of lift-curve inclination for NACA 0012 section at $M_\infty = 0.67$ and 0.75 as computed by FLO 36 and FLO 52MG.

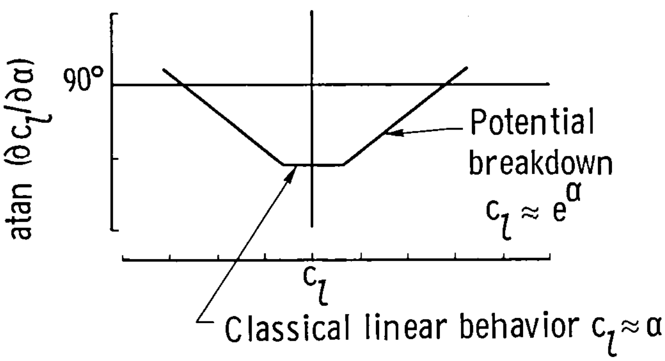

Figure 9. Sketch of variation of lift-curve inclination with lift coefficient (constant M_∞).

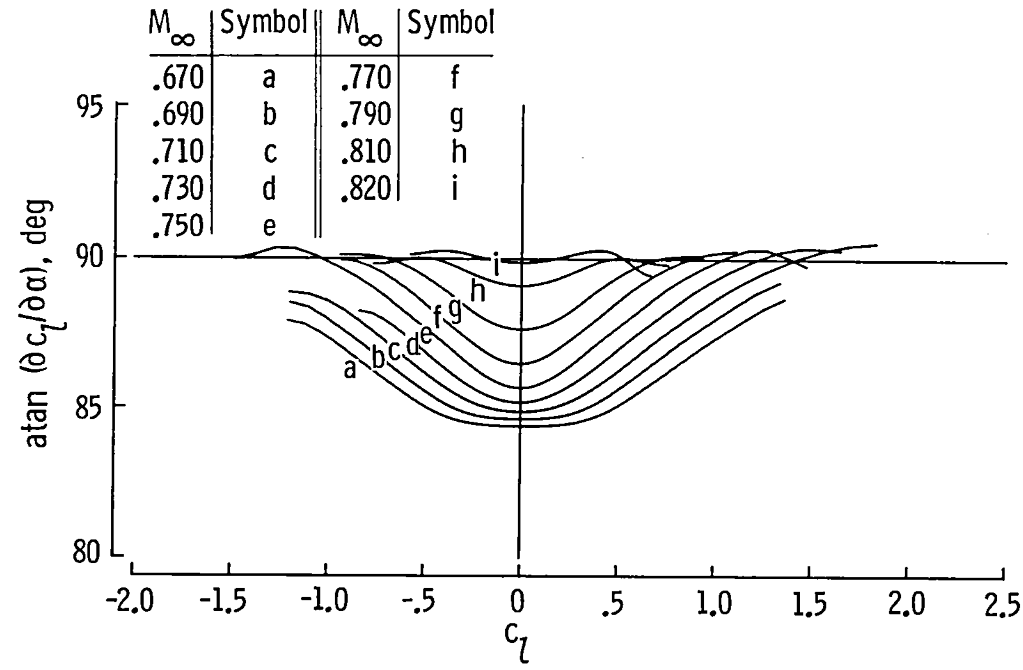

(a) NACA 0012.

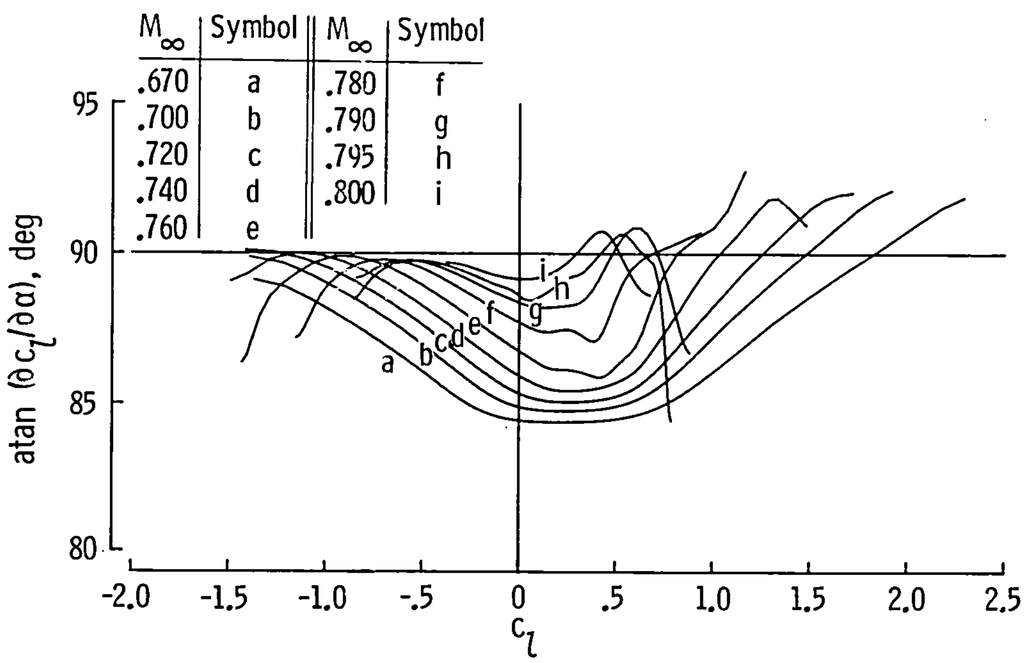

(b) KORN 75-06-12.

Figure 10. Behavior of lift-curve inclination computed with FLO 36.

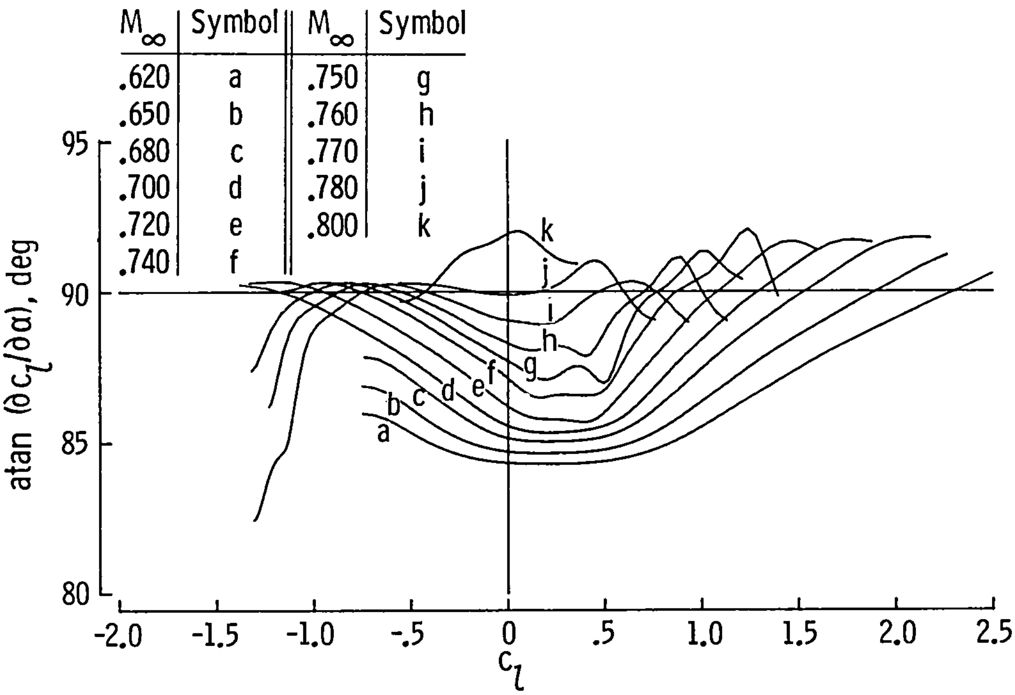

(c) NLR 7301.

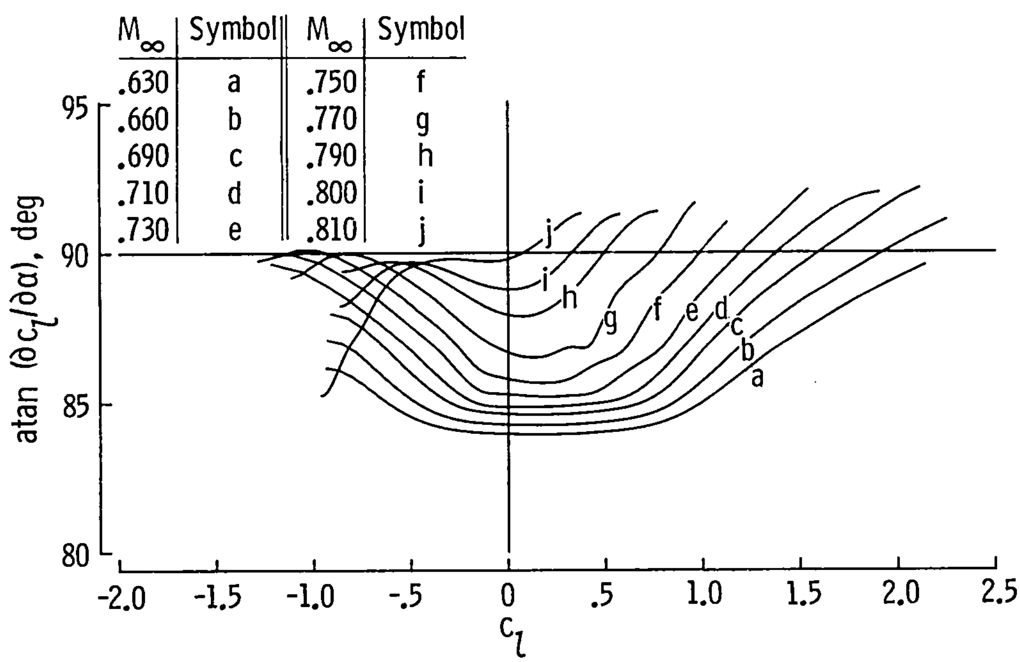

(d) RAE 2822.

Figure 10. Continued.

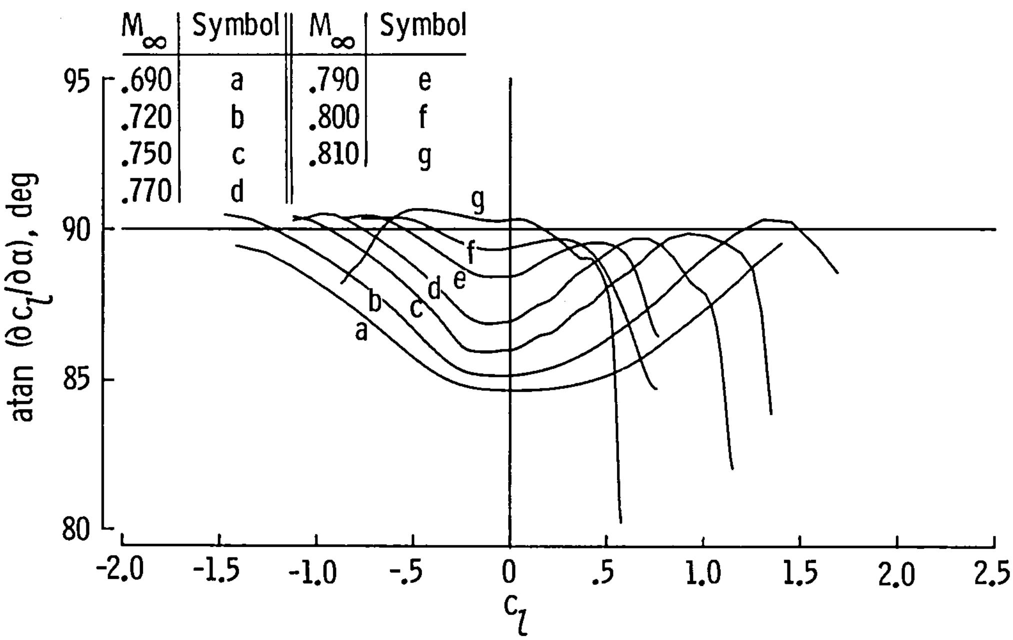

(e) NACA 65-213.

Figure 10. Concluded.

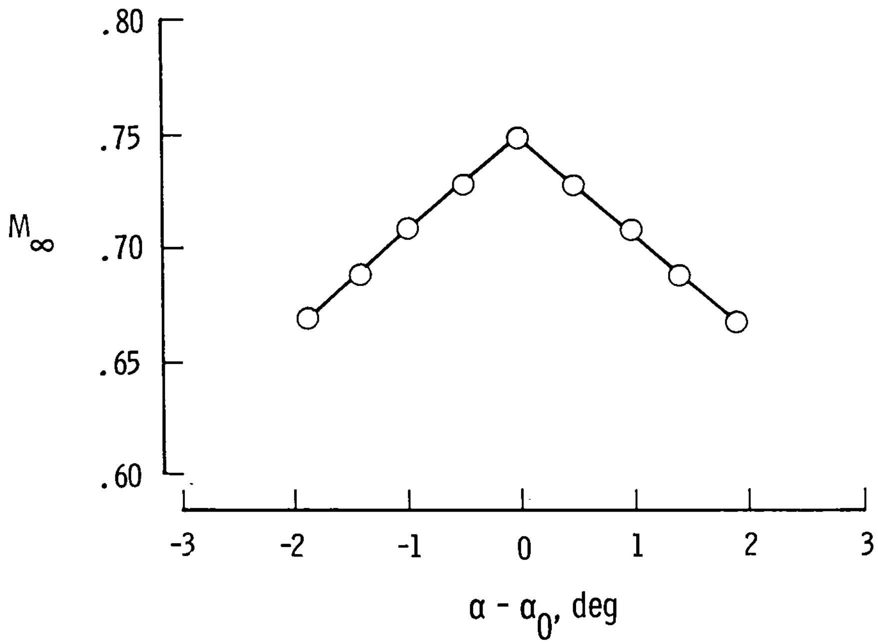

(a) NACA 0012.

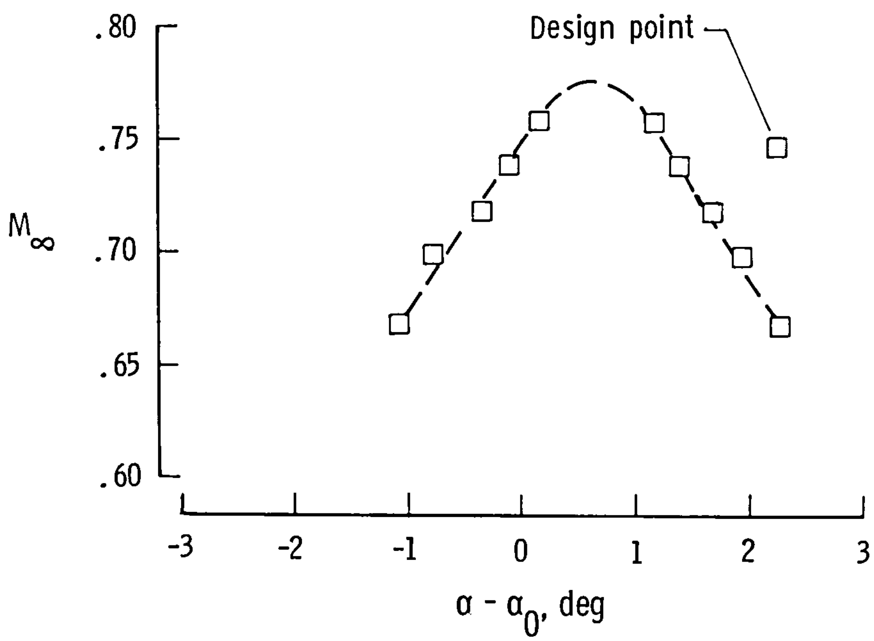

(b) KORN 75-06-12.

Figure 11. Location in α, M_∞ plane where conservative potential approximation begins to break down. Design points for NLR 7301 and KORN 75-06-12 airfoil sections are indicated on the figures.

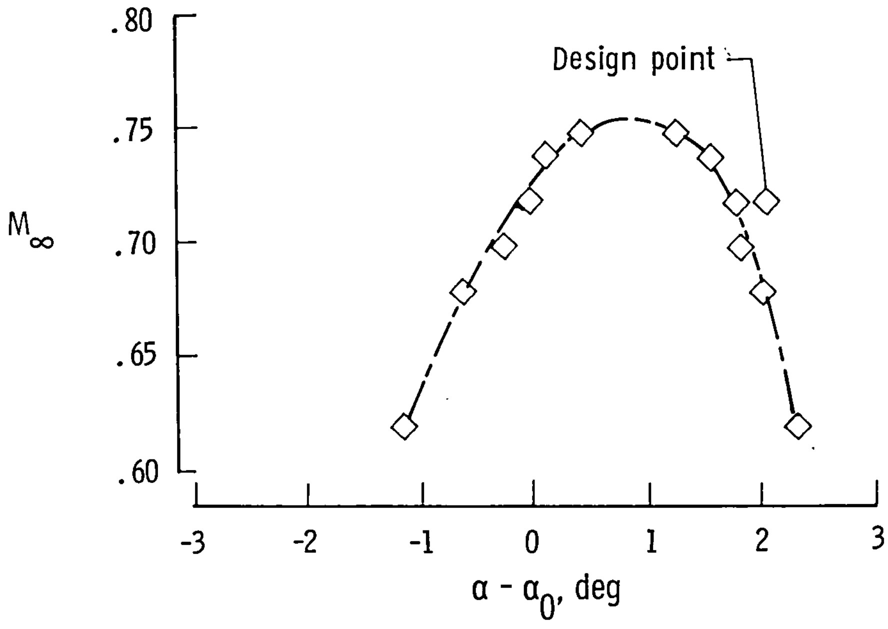

(c) NLR 7301.

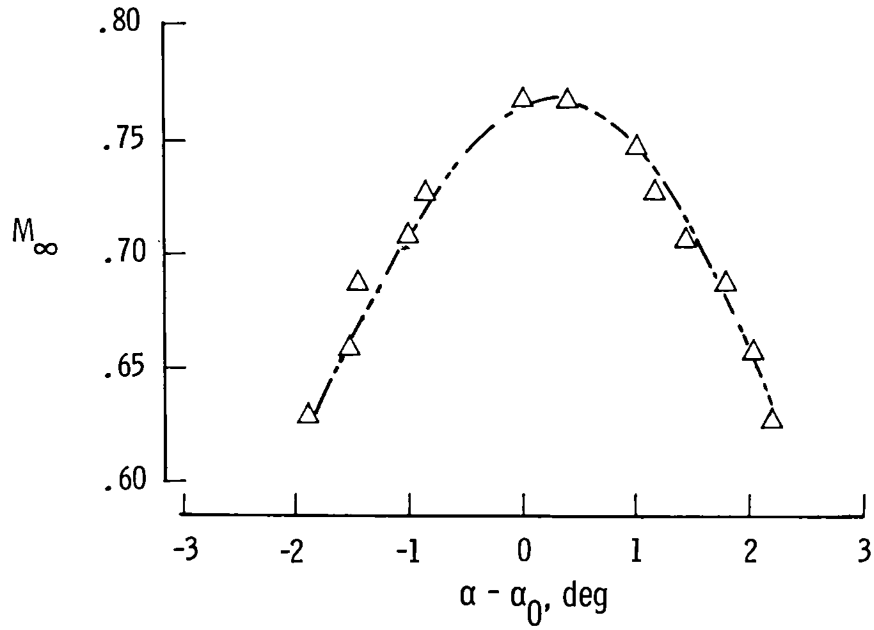

(d) RAE 2822.

Figure 11. Continued.

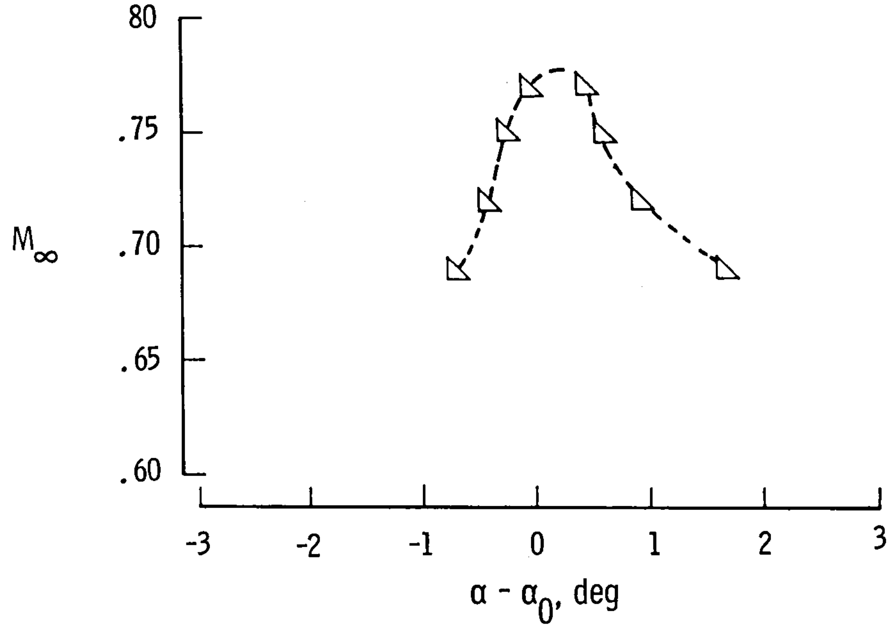

(e) NACA 65-213.

Figure 11. Concluded.

Standard Bibliographic Page

1. Report No.	2. Government Accession No.	3. Recipient's Catalog No.
NASA TP-2539		

4. Title and Subtitle
Breakdown of the Conservative Potential Equation

5. Report Date
February 1986

6. Performing Organization Code
505-60-01-01

7. Author(s)
M. D. Salas and Clyde R. Gumbert

8. Performing Organization Report No.
L-15769

9. Performing Organization Name and Address
NASA Langley Research Center
Hampton, VA 23665-5225

10. Work Unit No.

11. Contract or Grant No.

12. Sponsoring Agency Name and Address
National Aeronautics and Space Administration
Washington, DC 20546-0001

13. Type of Report and Period Covered
Technical Paper

14. Sponsoring Agency Code

15. Supplementary Notes
Information included in this report was released previously in AIAA Paper 85-0367 presented at the AIAA 23rd Aerospace Sciences Meeting, Reno, Nevada, January 14-17, 1985.

16. Abstract
The conservative full-potential equation is used to study transonic flow over five airfoil sections. The results of the study indicate that once shock waves are present in the flow, the qualitative behavior of the potential approximation is different from that observed with the Euler equations. The difference in behavior for the potential equation approximation eventually leads to multiple solutions. A map of the region in the angle-of-attack, Mach number (α, M_∞) plane showing where the conservative potential model begins to deviate from the Euler model is presented for the five airfoils investigated.

17. Key Words (Suggested by Authors(s))
Conservative potential equations
Transonic flow
Inviscid flow

18. Distribution Statement
Unclassified—Unlimited

Subject Category 02

19. Security Classif.(of this report)	20. Security Classif.(of this page)	21. No. of Pages	22. Price
Unclassified	Unclassified	35	A03

For sale by the National Technical Information Service, Springfield, Virginia 22161

NASA-Langley, 1986

National Aeronautics and
Space Administration
Code NIT-4

Washington, D.C.
20546-0001

NASA